Frontiers of Computational Fluid Dynamics – 2004

David A. Caughey & Mohamed M. Hafez, Eds.

2004

Chapter 1

Control of Flow Separation over a Circular Cylinder Using Electro-Magnetic Fields: Numerical Simulation

Brian H. Dennis[1] and George S. Dulikravich[2]

1.1 Nomenclature

$\underline{B} = \mu_0(\underline{H} + \underline{M})$	magnetic flux density, $kg\ A^{-1}\ s^{-2}$
C_p	specific heat at constant pressure, $K^{-1}\ m^2\ s^{-2}$
$\underline{\underline{d}} = \frac{1}{2}[\nabla \underline{v} + (\nabla \underline{v})^T]$	average rate of deformation tensor, s^{-1}
$\frac{D}{Dt} = \frac{\partial}{\partial t} + \underline{v} \cdot \nabla$	material derivative, s^{-1}
$\underline{D} = \epsilon_0 \underline{E} + \underline{P}$	electric displacement vector, $A\ s\ m^{-2}$
$\underline{E}$	electric field intensity, $kg\ m\ s^{-3}\ A^{-1}$
$\underline{\hat{E}} = \underline{E} + \underline{v} \times \underline{B}$	electromotive intensity, $kg\ m\ s^{-3}\ A^{-1}$
$\underline{H}$	magnetic field intensity, $A\ m^{-1}$
$\underline{\underline{I}}$	unit tensor
$\underline{J} = \underline{J_c} + q_e \underline{v}$	electric current density, $A\ m^{-2}$
$\underline{J_c}$	electric conduction current, $A\ m^{-2}$
$\underline{M}$	total magnetization per unit volume, $A\ m^{-1}$
$\underline{\hat{M}} = \underline{M} + \underline{v} \times \underline{P}$	magnetomotive intensity, $A\ m^{-1}$

[1]Mechanical and Aerospace Engineering, University of Texas at Arlington, Arlington, Texas, 76019
[2]Mechanical and Materials Engineering, Florida International University, 10555 W. Flagler St., Miami, FL, U.S.A. 33174

p	pressure, $kg\ m^{-}1\ s^{-2}$
$\underline{P}$	total polarization per unit volume, $A\ s\ m^{-2}$
q_e	total electric charge per unit volume, $A\ s\ m^{-3}$
$\underline{q}$	conduction heat flux, $kg\ s^{-3}$
Q_h	heat source per unit volume, $kg\ m^{-1}\ s^{-3}$
t	time, s
$\underline{\underline{t}} = -\varphi \underline{\underline{I}} + \underline{\underline{\tau}}$	Cauchy stress tensor, $kg\ m^{-1}\ s^{-2}$
T	absolute temperature, K
$\hat{u}$	internal energy per unit mass, $m^2\ s^{-2}$
$\underline{v}$	fluid velocity,$m\ s^{-1}$
Greek Symbols	
ϵ	electric permittivity, $kg^{-1}\ m^{-3}\ s^4\ A^2$
ϵ_0	electric permittivity of vacuum, $kg^{-1}\ m^{-3}\ s^4\ A^2$
$\epsilon_p = \epsilon_0 \chi_e$	polarization electric permittivity, $kg^{-1}\ m^{-3}\ s^4\ A^2$
$\epsilon_r = \epsilon / \epsilon_0$	relative electric permittivity
η	fluid viscosity, $kgm^{-1}s^{-1}$
ϕ	electric potential, Vm
φ	modified hydrostatic pressure, $kgm^{-1}s^{-2}$
ρ	fluid density, $kg\ m^{-3}$
$\underline{\underline{\tau}}$	deviator part of stress tensor, $kg\ m^{-1}\ s^{-2}$
μ	magnetic permeability, $kg\ m\ A^{-2}\ s^{-2}$
$\mu_0 = 4\pi \times 10^{-7}$	magnetic permeability of vacuum, $kg\, mA^{-2}s^{-2}$
$\mu_r = \mu / \mu_0$	relative magnetic permeability
$\mu_m = \mu_0 / \chi_B$	magnetization magnetic permeability,$kg\, mA^{-2}s^{-2}$
$\chi_B = 1 - \mu_r^{-1}$	magnetic susceptibility based on B
$\chi_e = \epsilon_r - 1$	electric susceptibility
$\underline{\omega}$	vorticity, s^{-1}

1.2 Introduction

In recent years there has been a growing interest in the simulation of coupled physics or multidisciplinary phenomena. Advances in computer processor technology has recently allowed researchers to consider large systems of differential equations representing complex coupled problems. An example of a multidisciplinary analysis is the simulation of fluid flow under the influence of externally applied electro-magnetic fields. The study of fluid flows containing electric charges under the influence of an externally applied electric field and negligible magnetic field is known as electrohydrodynamics or EHD. The study of fluid flows without electric charges and influenced only by an externally applied magnetic field is known as magnetohydrodynamics or MHD [18]. Numerous publications are available dealing with the EHD and the MHD models [19, 13], their numerical simulations, and applications [6, 4, 3, 5, 7, 17, 9, 8, 1]. Although fairly complex, the existing mathematical models for EHD and MHD often

represent unacceptably simplified and inconsistent models of the actual physics [11]. The study of fluid flows under the combined influence of the externally applied and internally generated electric and magnetic fields is often called electro-magneto-fluid dynamics (EMFD) [12, 10]. However, the mathematical model for such combined electromagnetic field interaction with fluid flows is extremely complex and requires a large number of new physical properties of the fluid that cannot be found in open literature. Thus, a somewhat simplified mathematical model should be used in actual numerical simulations of fluid flows under the combined influence of the externally applied electric and magnetic fields. In the case of incompressible fluids, such a non-linear model termed second order lectromagnetohydrodynamics (EMHD) was derived by Ko and Dulikravich [15]. This is a second order theory that is fully consistent with all of the basic assumptions of the complete EMFD model [12, 10]. The basic assumptions are that the electric and magnetic fields, rate of strain, and temperature gradient are relatively small. Furthermore, terms of second order and higher in the average rate of deformation tensor are neglected as in the case of conventional Newtonian fluids. Only the terms up to second order in $\underline{\underline{d}}, \underline{\underline{\hat{E}}}, \underline{B}, \nabla T$ are retained. Because of the unavailability of the complete EMHD model until recently and because of the considerable complexity of even simpler versions of the EMHD model, it is still hard to find publications dealing with the combined influence of electric and magnetic fields and fluid flow.

The objective of this paper is to present numerical results for the flow over a circular cylinder that is under the influence of combined electric and magnetic fields. The results presented here indicate that electro-magnetic fields can be used to eliminate the flow separation in steady flow. In addition, results also show that electro-magnetic fields can be used to eliminate periodic vortex shedding in the case of unsteady flow. These simulations were performed using a simplified EMHD model for the case of two-dimensional planar flows for electrically conducting incompressible fluids. The equations were discretized with the Least-Squares Finite Element Method (LSFEM) and solved on a single processor workstation. The numerical results will be presented for both steady and unsteady laminar flows of homocompositional Newtonian fluids. The accuracy of the numerical method was also verified against a simple analytical solution for magnetohydrodynamics.

It should be pointed out that similar effects on the flow-field around a circular cylinder were numerically predicted and experimentally verified by a research team from Germany [20, 21]. However, their arrangement of magnets and electrodes was entirely different from the arrangement presented in this paper indicating that there are multiple configurations of magnets and electrodes capable of producing the same flow-field alterations.

1.3 Second Order Analytical Model of EMHD

A full system of partial differential equations governing incompressible flows under the combined effects of electromagnetic forces [15] is summarized in this section by using the constitutive equations which have been derived through the second order theory.

Specifically, polarization and magnetization vectors are defined as

$$\underline{P} = \epsilon_0 \chi_e \hat{\underline{E}} \equiv \epsilon_p \underline{\hat{E}}, \;\; \underline{\hat{M}} = \frac{\chi_B}{\mu_0} \underline{B} \equiv \frac{\underline{B}}{\mu_m}. \tag{1.1}$$

which indicates a medium with purely instantaneous response [16]. The deviator part of the stress tensor is defined as

$$\begin{array}{c} \underline{\underline{\tau}} = 2\mu_v \underline{\underline{d}} - \sigma_2 \hat{\underline{E}} \otimes \hat{\underline{E}} - T^{-1}\kappa_2 \nabla T \otimes \nabla T \\ -(T^{-1}\kappa_5 + \sigma_5)(\hat{\underline{E}} \cdot \nabla T)_S, \end{array} \tag{1.2}$$

Electric current conduction vector is defined as

$$\begin{array}{c} \underline{J_c} = \sigma_1 \hat{\underline{E}} + \sigma_2 \underline{\underline{d}} \cdot \hat{\underline{E}} + \sigma_4 \nabla T + \sigma_5 \underline{\underline{d}} \cdot \nabla T \\ +\sigma_7 \hat{\underline{E}} \times \underline{B} + T^{-1}\kappa_8 \nabla T \times \underline{B}, \end{array} \tag{1.3}$$

while thermal conduction flux is defined as

$$\underline{q} = \kappa_1 \nabla T + \kappa_2 \underline{\underline{d}} \cdot \nabla T + \kappa_4 \hat{\underline{E}} + \kappa_7 \nabla \times \underline{B} + \kappa_8 \hat{\underline{E}} \times \underline{B}, \tag{1.4}$$

Then, Maxwell's equations become

$$\nabla \cdot \left(\epsilon_0 \underline{E} + \epsilon_p \hat{\underline{E}} \right) = q_e, \tag{1.5}$$

$$\nabla \cdot \underline{B} = 0, \tag{1.6}$$

$$\nabla \times \underline{E} = \frac{\partial \underline{B}}{\partial t}, \tag{1.7}$$

$$\begin{aligned} \nabla \times \left(\frac{\underline{B}}{\mu} + \epsilon_p \underline{v} \times \hat{\underline{E}} \right) &= \frac{\partial}{\partial t} \left(\epsilon_0 \underline{E} + \epsilon_p \hat{\underline{E}} \right) \\ &+ q_e \underline{v} + \sigma_1 \hat{\underline{E}} + \sigma_2 \underline{\underline{d}} \cdot \hat{\underline{E}} + \sigma_4 \nabla T \\ &+ \sigma_5 \underline{\underline{d}} \cdot \nabla T + \sigma_7 \hat{\underline{E}} \times \underline{B} + T^{-1}\kappa_8 \nabla T \times \underline{B}. \end{aligned} \tag{1.8}$$

while the Navier-Stokes equations become

$$\nabla \cdot \underline{v} = 0, \tag{1.9}$$

$$\begin{aligned} \rho \frac{D\underline{v}}{Dt} &= -\rho g [1 - \alpha(T - T_0)] \underline{i_3} - \nabla \left(p + p_e + p_m \right) \\ &+ \nabla \cdot \left(\mu_v \left(\nabla \underline{v} + \nabla \underline{v}^T \right) \right) - \nabla \cdot \left(\sigma_2 (\hat{\underline{E}} \otimes \hat{\underline{E}}) \right) \\ &- \nabla \cdot \left(T^{-1}\kappa_2 \left(\nabla T \otimes \nabla T \right) \right) + q_e \hat{\underline{E}} \\ &- \nabla \cdot \left((T^{-1}\kappa_5 + \sigma_5)(\hat{\underline{E}} \otimes \nabla T)_S \right) + \sigma_1 \hat{\underline{E}} \times \underline{B} \\ &+ \sigma_2 \underline{\underline{d}} \cdot \hat{\underline{E}} \times \underline{B} + \sigma_4 \nabla T \times \underline{B} + \sigma_5 \underline{\underline{d}} \cdot \nabla T \times \underline{B} \\ &+ \sigma_7 (\hat{\underline{E}} \times \underline{B}) \times \underline{B} + T^{-1}\kappa_8 (\nabla T \times \underline{B}) \times \underline{B} \end{aligned} \tag{1.10}$$

$$
\begin{aligned}
&+ \quad \epsilon_p(\nabla \underline{E}) \cdot \hat{\underline{E}} + (\nabla \underline{B}) \cdot (\frac{\underline{B}}{\mu_m} - \epsilon_p \underline{v} \times \hat{\underline{E}} + \frac{D}{Dt}(\epsilon_p \hat{\underline{E}} \times \underline{B})), \\
\rho C_p \frac{DT}{Dt} &= Q_h + \nabla \cdot (\kappa_1 \nabla T + \kappa_2 \underline{\underline{d}} \cdot \nabla T + \kappa_4 \hat{\underline{E}} + \kappa_5 \underline{\underline{d}} \cdot \underline{E} \\
&+ \quad \kappa_7 \nabla T \times \underline{B} + \kappa_8 \underline{E} \cdot \underline{B}) + \sigma_1 \hat{\underline{E}} \cdot \hat{\underline{E}} + \sigma_4 \hat{\underline{E}} \cdot \nabla T \\
&- \quad \frac{\kappa_2}{T} \nabla T \cdot \underline{\underline{d}} \cdot \nabla T - \frac{\kappa_5}{T} \hat{\underline{E}} \cdot \underline{\underline{d}} \cdot \nabla T + \frac{\kappa_8}{T} \hat{\underline{E}} \cdot (\nabla T \times \underline{B}) \\
&+ \quad \hat{\underline{E}} \cdot \frac{D(\epsilon \hat{\underline{E}})}{Dt} - \frac{\underline{B}}{\mu_m} \cdot \frac{D\underline{B}}{Dt}.
\end{aligned}
\tag{1.11}
$$

Notice that in this EMHD model the physical properties of the incompressible fluid, χ_e, χ_B, μ_v, σ_1, σ_2, σ_4, σ_5, σ_7, κ_1, κ_2, κ_4, κ_5, κ_7, κ_8, α, can be either constants or functions of temperature only.

1.4 Least-Squares Finite Element Method

The system of partial differential equations described in this section 1.3 is discretized using the Least-Squares Finite Element Method (LSFEM). We first look at the LSFEM for a general linear first-order system [14, 2]

$$\underline{\underline{L}} \underline{u} = \underline{f} \tag{1.12}$$

where

$$\underline{\underline{L}} = \underline{\underline{A_1}} \frac{\partial}{\partial x} + \underline{\underline{A_2}} \frac{\partial}{\partial y} + \underline{\underline{A_3}} \tag{1.13}$$

for two-dimensional problems. The residual of the system is represented by $\underline{R}$.

$$\underline{R}(\underline{u}) = \underline{\underline{L}} \underline{u} - \underline{f} \tag{1.14}$$

We now define the following least squares functional I over the domain Ω

$$I(\underline{u}) = \int_\Omega \underline{R}(\underline{u})^T \cdot \underline{R}(\underline{u}) \, dx \, dy \tag{1.15}$$

The weak statement is then obtained by taking the variation of I with respect to $\underline{u}$ and setting the result equal to zero.

$$\delta I(\underline{u}) = \int_\Omega \left(\underline{\underline{L}} \delta \underline{u}\right) \left(\underline{\underline{L}} \underline{u} - \underline{f}\right) dx \, dy = 0 \tag{1.16}$$

Using equal order shape functions, $\underline{\hat{\phi}}_i$, for all unknowns, the vector $\underline{u}$ is written as

$$\underline{u} = \sum_{i=1}^{n} \underline{\hat{\phi}}_i \left\{ u_1, u_2, u_3, ..., u_m \right\}_i^T \tag{1.17}$$

where $\{u_1, u_2, u_3, ..., u_m\}_i$ are the nodal values at the ith node of the finite element. Introducing the above approximation for $\underline{u}$ into the weak statement leads to a linear system of algebraic equations

$$\underline{\underline{K}}\,\underline{U} = \underline{F} \tag{1.18}$$

where $\underline{\underline{K}}$ is the stiffness matrix, $\underline{U}$ is the vector of unknowns, and $\underline{F}$ is the force vector.

1.4.1 Nondimensional First Order Form for Simplified EMHD

The full system of partial differential equations describing EMHD flows contain many parameters that refer to physical properties that are not known at this time. Rather than complete numerical simulations with guessed values of these parameters, we chose to work with only those terms for which the material properties are known. In this case, we simplify the equations by retaining only source terms that contain κ_1 and σ_1 since these values are available for various fluids.

Use of LSFEM for systems of equations that contain higher order derivatives is usually difficult due to the higher continuity restrictions imposed on the approximation functions. For this reason it is more convenient to transform the system into an equivalent first order form before applying LSFEM. For the case of electro-magneto-hydrodynamics, the second order derivatives are transformed by introducing vorticity, $\underline{\omega}$, as an additional unknown.

In addition, we assume the flow is unsteady but isothermal and without charged particles. In this case the energy and charge transport equations are not required and source terms associated with charges are dropped. We also consider only electrostatic and magnetostatic fields.

$$\nabla \cdot \underline{v}^* = 0 \tag{1.19}$$

$$\frac{\partial \underline{v}^*}{\partial t} + \underline{v}^* \cdot \nabla \underline{v}^* + \frac{1}{Re}\nabla \times \underline{\omega}^* + \nabla p^* - \frac{Ht^2}{Re}\underline{v}^* \times \underline{B}^* \times \underline{B}^* - M_1 \underline{E}^* \times \underline{B}^* = 0 \tag{1.20}$$

$$\underline{\omega}^* - \nabla \times \underline{v}^* = 0 \tag{1.21}$$

$$\nabla \cdot \underline{B}^* = 0 \tag{1.22}$$

$$\nabla \times \underline{B}^* = Rm\underline{v^*} \times \underline{B}^* + B_2 \underline{E}^* \tag{1.23}$$

$$\nabla \cdot \underline{E}^* = 0 \tag{1.24}$$

$$\nabla \times \underline{E}^* = 0 \tag{1.25}$$

$$\nabla \phi^* = \underline{E}^* \tag{1.26}$$

where $\underline{v}^* = \underline{v}\, v_0^{-1}$, $\underline{\omega}^* = \underline{\omega}\, L_0 v_0^{-1}$, $\underline{B}^* = \underline{B}\, B_0^{-1}$, $\underline{E}^* = \underline{E} L_0\, \Delta\phi_0^{-1}$,$\phi^* = \phi \Delta\phi_0^{-1}$, $p^* = p\, \rho^{-1} v_0^{-2}$, $x^* = x\, L_0^{-1}$, $y^* = y\, L_0^{-1}$. Here, L_0 is the reference length, v_0 is the reference speed, $\Delta\phi_0$ is the reference electric potential difference, and B_0 is the reference magnetic flux density. For convenience the $*$ superscript will be dropped for the remainder of the paper.

The nondimensional numbers are given by:

$$Rm = \mu\sigma v_0 L_0 \ , \quad B_2 = \frac{\mu_0\sigma_0\Delta\phi_0}{B_0} \ , \quad Re = \frac{\rho_0 v_0 L_0}{\eta_0} \ , \quad Ht = L_0 B_0\sqrt{\frac{\sigma_0}{\eta_0}} \ , \quad M_1 = \frac{\Delta\phi_0 B_0\sigma_0}{\rho_0 v_0^2} \tag{1.27}$$

It should be noted that the electric potential is introduced as an additional variable due to the convenience of applying physically meaningful boundary conditions for electrodes. For the electric field equations, the first order form of Maxwell's equations does not include electric potential. Since the most common boundary conditions for static electric fields are given in terms of potential, it is necessary to add the equation (1.26) for electric potential, ϕ.

We now write the above system in the general form of a first-order system (1.12). Although the entire system written in (1.19)-(1.26) can be treated by LSFEM, it was found to be more economical to solve the fluid and electromagnetic field equations separately, in an iterative manner. Here, a general form first order system is written for the fluid system (1.19)- (1.21) and denoted by the superscript $fluid$. Here the time derivative term in the fluid equations is approximated using the backward-Euler scheme.

$$\frac{\partial \underline{v}}{\partial t} \approx \frac{\underline{v}^{n+1} - \underline{v}^{n}}{\Delta t} \tag{1.28}$$

A first-order system is also written in general form for the electro-magnetic field equations (1.22)-(1.26) and is denoted by the superscript em. In addition, the nonlinear convective terms in the fluid equations are linearized with Newton's method leading to a system suitable for treatment with the LSFEM. For the two-dimensional case we specify the z component of the magnetic field and assume the x and y components are zero. For many engineering applications, the magnitude of Rm and B_2 is typically small so we expect the current-induced magnetic field in $x-y$ to be negligible compared to the magnitude of the externally applied magnetic field. The x and y components for velocity, $\underline{v}$, and electric field, $\underline{E}$, are left as unknowns while their z components are assumed to be zero. For simplicity, we only consider flows that do not contain free charged particles.

$$\underline{\underline{A}}_1^{fluid} = \begin{bmatrix} 1 & 0 & 0 & 0 \\ u_0 & 0 & 1 & 0 \\ 0 & u_0 & 0 & -\frac{1}{Re} \\ 0 & -1 & 0 & 0 \end{bmatrix}, \qquad \underline{\underline{A}}_2^{fluid} = \begin{bmatrix} 0 & 1 & 0 & 0 \\ v_0 & 0 & 0 & \frac{1}{Re} \\ 0 & v_0 & 1 & 0 \\ 1 & 0 & 0 & 0 \end{bmatrix},$$

$$\underline{\underline{A}}_3^{fluid} = \begin{bmatrix} 0 & 0 & 0\,0 \\ \frac{1}{\Delta t} + \frac{Ht^2}{Re}B_{z0}^2 + \frac{\partial u_0}{\partial x} & \frac{\partial u_0}{\partial y} & 0\,0 \\ \frac{\partial v_0}{\partial x} & \frac{1}{\Delta t} + \frac{Ht^2}{Re}B_{z0}^2 + \frac{\partial v_0}{\partial y} & 0\,0 \\ 0 & 0 & 0\,1 \end{bmatrix},$$

$$\underline{f}^{fluid} = \begin{Bmatrix} 0 \\ \frac{u^n}{\Delta t} + u_0 \frac{\partial u_o}{\partial x} + v_0 \frac{\partial u_o}{\partial y} - M_1 E_{y_0} B_{z_0} \\ \frac{v^n}{\Delta t} + u_0 \frac{\partial v_o}{\partial x} + v_0 \frac{\partial v_o}{\partial y} + M_1 E_{x_0} B_{z_0} \\ 0 \end{Bmatrix}, \quad \underline{u}^{fluid} = \begin{Bmatrix} u \\ v \\ p \\ \omega \end{Bmatrix}^{n+1} \tag{1.29}$$

$$\underline{\underline{A}}_1^{em} = \begin{bmatrix} 0 & 1 & 0 \\ 1 & 0 & 0 \\ 0 & 0 & 0 \\ 0 & 0 & -1 \end{bmatrix}, \quad \underline{\underline{A}}_2^{em} = \begin{bmatrix} 0 & 0 & 1 \\ 0 & 0 & 0 \\ 1 & 0 & 0 \\ 0 & 1 & 0 \end{bmatrix}, \quad \underline{\underline{A}}_3^{em} = \begin{bmatrix} 0 & 0 & 0 \\ 0 & -1 & 0 \\ 0 & 0 & -1 \\ 0 & 0 & 0 \end{bmatrix},$$

$$\underline{f}^{em} = \begin{Bmatrix} 0 \\ 0 \\ 0 \\ 0 \end{Bmatrix}, \; \underline{u}^{em} = \begin{Bmatrix} \phi \\ E_x \\ E_y \end{Bmatrix} \tag{1.30}$$

A solution satisfying all of the above systems of equations can be found by using a simple iterative process. First, the system given in (1.30) is solved for the electric field. The system in (1.29) is solved with the electric field and velocities from the previous time step. Here, quantities taken from the previous iteration are designated with the subscript 0. These equations may be iterated at each time step if the problem is very nonlinear. In that case the iteration at each time step is repeated until a specified convergence tolerance is reached. The reduction of the residual norm of both systems by 3.5 orders of magnitude is usually achieved in less than 5 iterations.

1.4.2 Verification of Accuracy

It is difficult to verify the accuracy of an EMHD code. This is due to the absence of analytical solutions for such equations. However, analytical solutions do exist for MHD flows. Here we will use such an analytic solution to validate the MHD portion of the code.

The accuracy of the LSFEM for MHD was tested against analytic solutions for Poiseuille-Hartmann flow [13]. The Poiseuille-Hartmann flow is a 1-D flow of a conducting and viscous fluid between two stationary plates with a uniform external magnetic field applied orthogonal to the plates. Assuming the walls are at $y = \pm L$ and that fluid velocity on the walls is zero and that the fluid moves in the x-direction under the influence of a constant pressure gradient, then the velocity profile is given by

$$u(y) = \frac{\rho H t}{\sigma B_y^2} \frac{\partial p}{\partial x} \left(\frac{\cosh(Ht) - \cosh(\frac{Hty}{L})}{\sinh(Ht)} \right) \tag{1.31}$$

The movement of the fluid induces a magnetic field in the x-direction and is given by

$$B_x(y) = \frac{B_y Rm}{Ht} \left(\frac{\sinh(\frac{Hty}{L}) - \frac{y}{L}\sinh(Ht)}{\cosh(Ht) - 1} \right) \tag{1.32}$$

A test case was run using the parameters given in Table 1.1 and with a mesh composed of 2718 parabolic triangular elements. Figure 1.1 shows the computed and analytical results for the velocity profile. Figure 1.2 shows the computed and analytical results for the induced magnetic field. For both cases, one can see that the agreement between the analytical solution and the LSFEM solution is excellent.

1.5 Numerical Results

The LSFEM formulation for EMHD will now be demonstrated for the electro-magnetic control of flow over a circular cylinder. The configuration of the electrodes and magnets is illustrated in Figure 1.3. In this configuration, the cylinder is divided into two electrodes, one on top and bottom, with magnets placed slightly downstream in the wake region. This configuration is in reality 3-D, but can be approximated in 2-D by specifying the z-component of the magnetic and computing the $x - y$ components of the electric and flow fields. The known magnetic field is assumed to be uniform and is applied into the $x - y$ plane.

The fluid is considered to be electrically conducting and flows over a circle with unit diameter. We computed both steady and unsteady flow cases to observe the effect of the electro-magnetic fields on the flow patterns. The relevant nondimensional parameters are shown in Table 1.2 for the two test cases.

The hybrid triangular and quadrilateral mesh shown in Figure 1.4 was used for all computations. The mesh is composed of 818 parabolic elements with 2458 nodes. No slip boundary conditions were applied to the cylinder surface while free stream conditions were applied at the inlet and top and bottom of the outer domain. Conditions on the outlet boundary were left free. Electric potentials are specified on the surfaces of the electrodes, thus creating a potential difference that forces current to flow through the electrically conducting fluid. Figure 1.5 shows the computed distribution of the electric potential as well as the electric field lines for the electrostatic field. The source terms in the EMHD system directly involve the electric field intensity, $\underline{E}$, so we expect that the shape of the field lines will have a strong influence on the flow pattern. In the present case, constant potentials are used on each electrode so the field lines are distributed smoothly across the domain.

In the first case, the steady flow at $Re = 37$ is computed with no electric or magnetic field. Figure 1.6 shows the streamlines and pressure distribution for this classical flow. When the electric and magnetic fields are applied to the flow, the velocity and pressure distribution has been changed dramatically as shown in Figure 1.7. One interesting note about this result is that although the separation behind the cylinder has been removed, the pressure on the back of the cylinder is significantly decreased. This low pressure is due to the increased flow velocity that occurs just behind the cylinder when the body force due to the electro-magnetic field is present. In addition, if the polarity of the electrodes is reversed, the opposite effect is observed. Figure 1.8 shows that the separation strength is actually enhanced by the reverse polarity electro-magnetic field. However, although the separation is stronger, the pressure on the back wall of the

cylinder increases. Once again, this increase in pressure is due to the energy inserted into the flow through the external electro-magnetic field.

In the second case, the unsteady flow at $Re = 100$ is first computed with no electric or magnetic field. The flow is computed from an initially uniform flow field until a periodic state is reached. For this case a time step $\Delta t = 0.1$ was used and the periodic flow was reached after 900 time steps. Figure 1.9 shows the particle traces at one instant around 1400 time steps. At this point the characteristic vortex shedding pattern can be clearly seen. The case was run again, but after 1200 time steps the static electro-magnetic field was activated. By 1400 time steps the particle traces in Figure 1.10 clearly show the effect of the electro-magnetic field on the wake structure. By the 2000 time step mark the flow reaches a steady, time-independent state. The flow becomes more stable due to the elimination of the periodic vortex shedding as shown in Figure 1.11. The combined electric and magnetic field in this configuration have a strong damping effect to the point of completely suppressing the vortex shedding typically seen at $Re = 100$. The resulting flow field is steady and is shown in Figure 1.12.

1.6 Conclusion

A unified theoretical model of simultaneously applied and interacting electric and magnetic fields and incompressible homocompositional viscous fluid flows has been expressed as a coupled sequence of first order partial differential equation systems. These systems were discretized in 2-D using a least-squares finite element method and integrated on an unstructured computational grid. Numerical results are in excellent agreement for the test case of a steady laminar flow between infinite parallel plates with simultaneously applied uniform vertical electric field and a uniform horizontal magnetic field. The method was used to simulate the flow over a circular cylinder with and without an externally applied electric and magnetic field. Results show that a certain arrangement of electrodes and magnets can be used to eliminate flow separations in steady flow and suppress vortex shedding in unsteady flows.

1.6.1 Acknowledgements

This work was performed while the primary author held the position of Visiting Associate Professor at the University of Tokyo. The primary author gratefully acknowledges support from the Graduate School of Frontier Sciences at the University of Tokyo. The second author is grateful for the partial support provided by the NSF grant DMS-0073698 administrated through the Computational Mathematics Program.

Bibliography

[1] M. J. Colaco, G. S. Dulikravich, and T. J. Martin. Optimization of wall electrodes for electro-hydrodynamic control of natural convection effects during solidification. *Materials and Manufacturing Processes*, 19(4), 2004.

[2] B. H. Dennis. *Simulation and Optimization of Electromagnetohydrodynamic Flows*. PhD thesis, Pennsylvania State University, University Park, PA, Dec. 2000.

[3] B. H. Dennis and G. S. Dulikravich. Magnetic field suppression of melt flow in crystal growth. *International Journal of Heat & Fluid Flow*, 23(3):pp. 269–277, 2002.

[4] B. H. Dennis, I. N. Egorov, Z.-X. Han, G. S. Dulikravich, and C. Poloni C. Multi-objective optimization of turbomachinery cascades for minimum loss, maximum loading, and maximum gap-to-chord ratio. *International Journal of Turbo & Jet-Engines*, 18(3):201–210, 2001.

[5] G. S. Dulikravich. Electro-magneto-hydrodynamics and solidification. In D. A. Siginer, D. De Kee, and R. P. Chhabra, editors, *Advances in Flow and Rheology of Non-Newtonian Fluids, Part B*, volume 8 of *Rheology Series*, chapter 9, pages 677–716. Elsevier Publishers, 1999.

[6] G. S. Dulikravich, V. Ahuja, and S. Lee. Modeling three-dimensional solidification with magnetic fields and reduced gravity. *International Journal of Heat and Mass Transfer*, 37(5):pp. 837–853, 1994.

[7] G. S. Dulikravich, K.-Y. Choi, and S. Lee. Magnetic field control of vorticity in steady incompressible laminar flows. In D. A. Siginer, J. H. Kim, S. A. Sheriff, and H. W. Colleman, editors, *Symposium on Developments in Electrorheological Flows and Measurement Uncertainty, ASME WAM'94*, 1994. Chicago, IL, Nov. 6-11, 1994, ASME FED-Vol. 205/AMD-Vol. 190, (1994), pp. 125-142.

[8] G. S. Dulikravich, M. J. Colaco, B. H. Dennis, T. J. Martin, I. N. Egorov-Yegorov, and S.-S. Lee. Optimization of intensities, and orientations of magnets controlling melt flow during solidification. *Materials and Manufacturing Processes*, 19(4):695–718, 2004.

[9] G. S. Dulikravich, M. J. Colaco, T. J. Martin, and S. Lee. Magnetized fiber orientation and concentration control in solidifying composites. *J. of Composite Materials*, 47(15):pp. 1351–1366, 2003.

[10] G. S. Dulikravich and S. R. Lynn. Unified electro-magneto-fluid dynamics (emfd): Introductory concepts. *International Journal of Non-Linear Mechanics*, 32(5):913–922, 1997.

[11] G. S. Dulikravich and S. R. Lynn. Unified electro-magneto-fluid dynamics (emfd): Survey of mathematical models. *International Journal of Non-Linear Mechanics*, 32(5):923–932, 1997.

[12] A. C. Eringen and G. A. Maugin. *Electrodynamics of Continua II; Fluids and Complex Media*. Springer-Verlag, New York, 1990.

[13] W. F. Hughes and F. J. Young. *The Electromagnetodynamics of Fluids*. John Wiley and Sons, New York, 1966.

[14] B-N. Jiang. *The Least-Squares Finite Element Method*. Spring-Verlag, Berlin, 1998.

[15] H.-J. Ko and G. S. Dulikravich. A fully non-linear model of electro-magneto-hydrodynamics. *International Journal of of Non-Linear Mechanics*, 35(4):pp. 709–719, 2000.

[16] A. Lakhtakia and W. S. Weiglhofer. On the causal constitutive relations of magnetoelectric media. In *1995 IEEE International Symposium on Electromagnetic Compatibility*. Atlanta, GA, August 14-18, (1995), pp. 611-613.

[17] A. J. Meir and P. G. Schmidt. Analysis and finite-element simulation of mhd flows, with an application to seawater drag reduction. In *Proceedings of the International Symposium on Seawater Drag Reduction, Newport, July 22 - 23*, pages 401–406, 1998.

[18] O.M. Stuetzer. Magnetohydrodynamics and electrohydrodynamics. *Physics of Fluids*, 5(5):534–544, 1962.

[19] G. W. Sutton and A. Sherman. *Engineering Magnetohydrodynamics*. McGraw Hill, New York, 1965.

[20] T. Weier, G. Gerbeth, G. Mutschke, O. Lielausis, and E. Platacis. Experiments on cylinder wake stabilization in an electrolyte solution by means of electromagnetic forces localized on the cylinder surface. *Experimental Thermal and Fluid Science*, 10:84–91, 1998.

[21] T. Weier, G. Gerbeth, O. Posdziech, O. Lielausis, and E. Platacis. Some results on electromagnetic control of flow around bodies. In *Proceedings of the International Symposium on Seawater Drag Reduction, Newport, July 22 - 23*, pages 395–400, 1998.

Table 1.1: Parameters used for Poisuille-Hartmann Flow Test Problem

Ht	10.0
Rm	6×10^{-7}
$L_0\,(m)$	1.0
$v_0\,(m\,s^{-1})$	0.6
$\eta\,(kg\,m^{-1}s^{-1})$	0.01
$B_0\,(T)$	1.0
$\mu\,(H\,m^{-1})$	1×10^{-6}
$\partial p/\partial x\,(Pa\,m^{-1})$	0.6
$\sigma\,(\Omega^{-1}m^{-1})$	1.0

Table 1.2: Non-dimensional numbers used for test cases

Number	Steady Case	Unsteady Case
Re	37.0	100.0
Ht	0.01	0.01
Rm	1.0×10^{-5}	1.0×10^{-5}
M_1	2.7	1.0

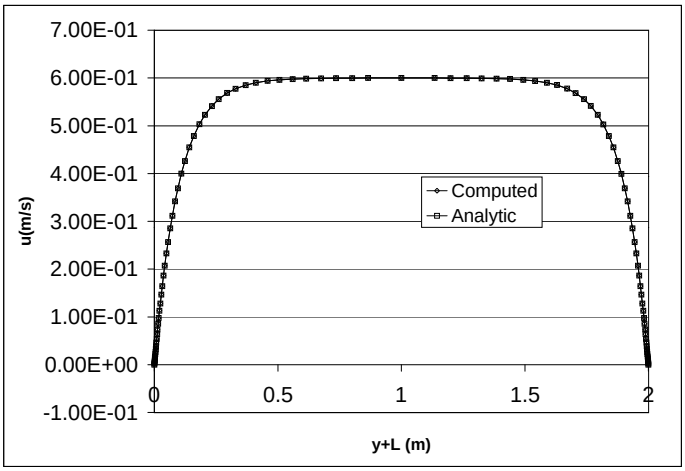

Figure 1.1: Computed and exact values for velocity

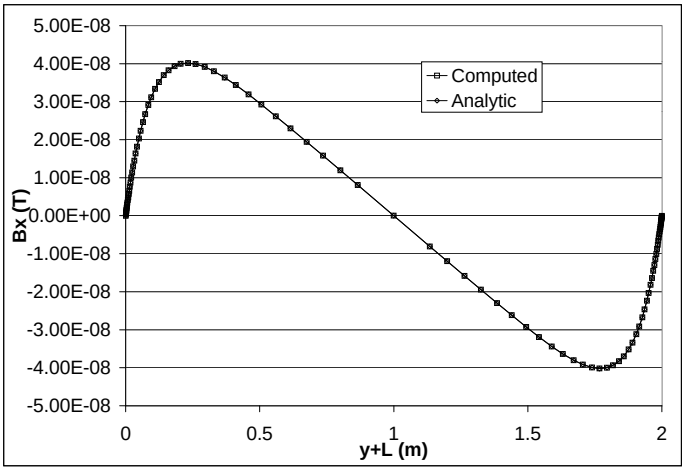

Figure 1.2: Computed and exact values for induced magnetic field

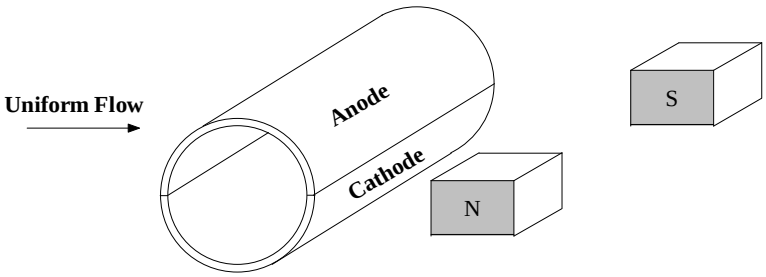

Figure 1.3: Test configuration for magnets and electrodes

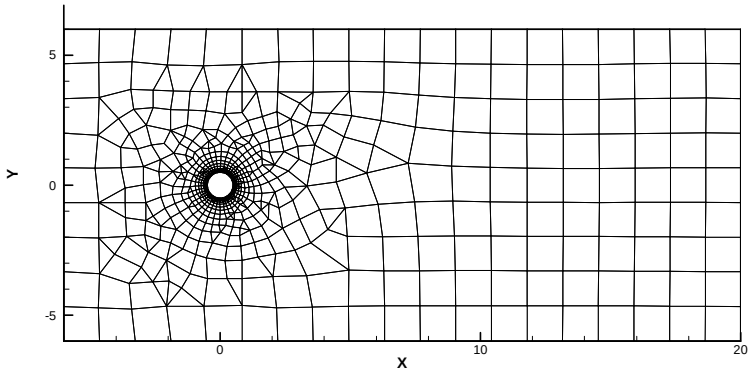

Figure 1.4: Hybrid unstructured mesh used

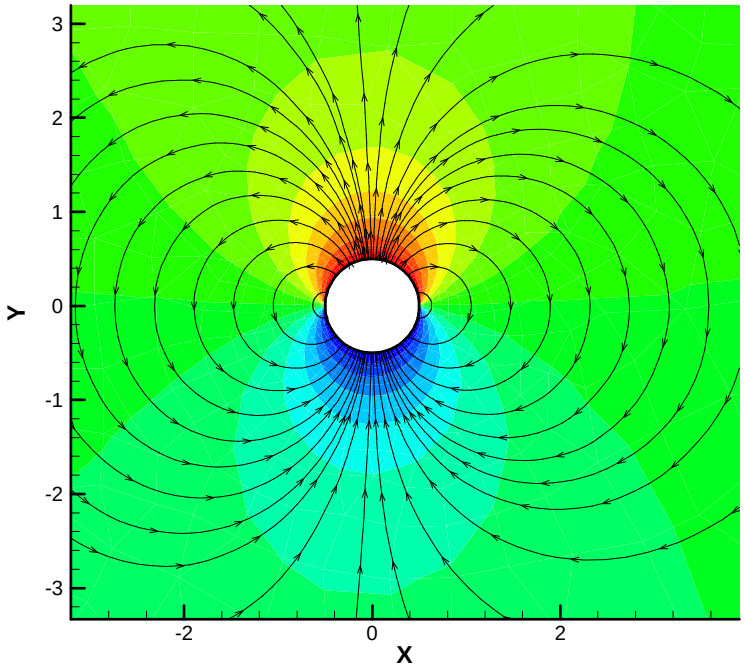

Figure 1.5: Computed electric field lines and electric potential contours

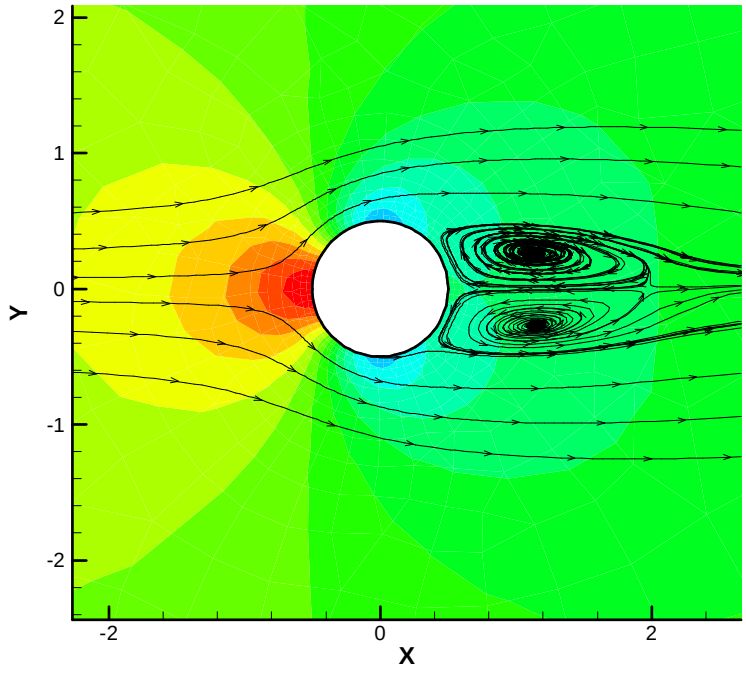

Figure 1.6: Pressure field and streamlines for steady flow with no electric field and no magnetic field

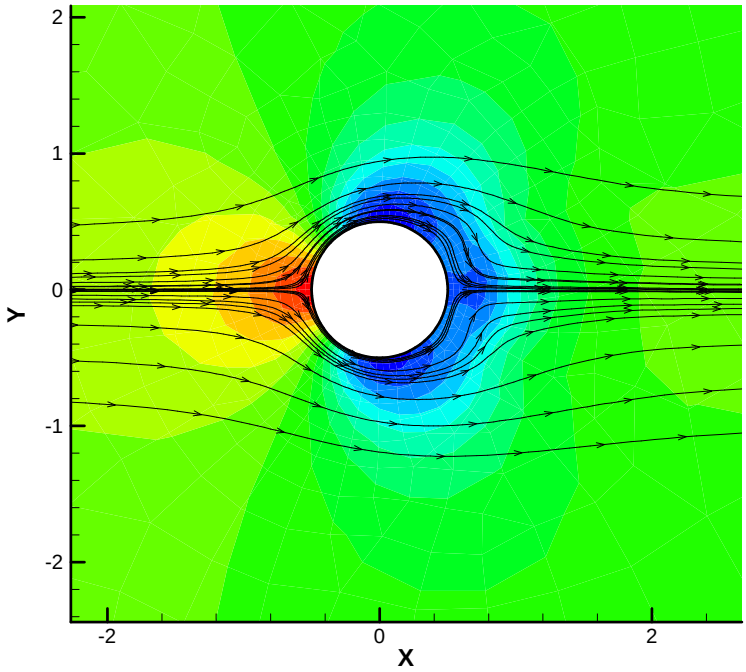

Figure 1.7: Pressure field and streamlines for steady flow with electric field and magnetic field

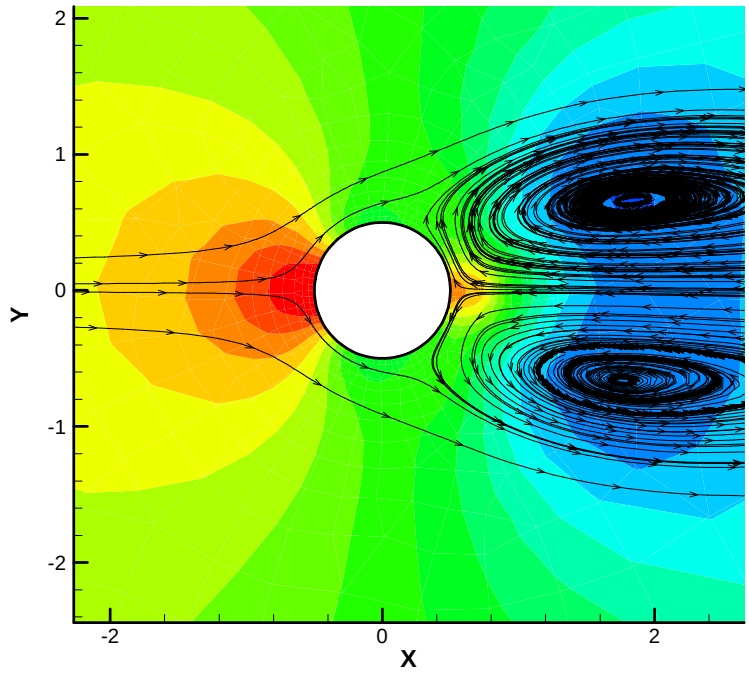

Figure 1.8: Pressure field and streamlines for steady flow with reversed electric field and magnetic field

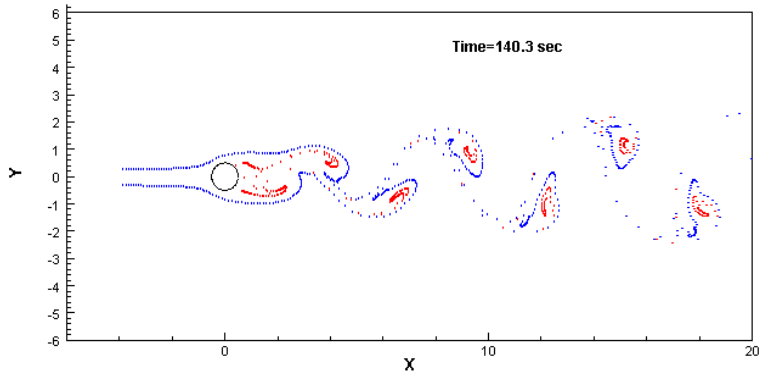

Figure 1.9: Particle traces for unsteady flow with no electric field and no magnetic field

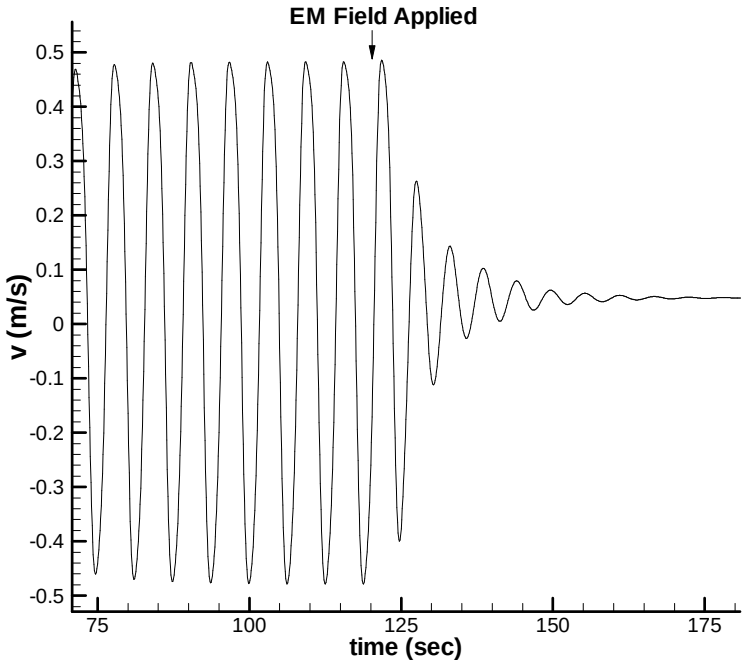

Figure 1.10: Time variation of v-component of velocity in the wake

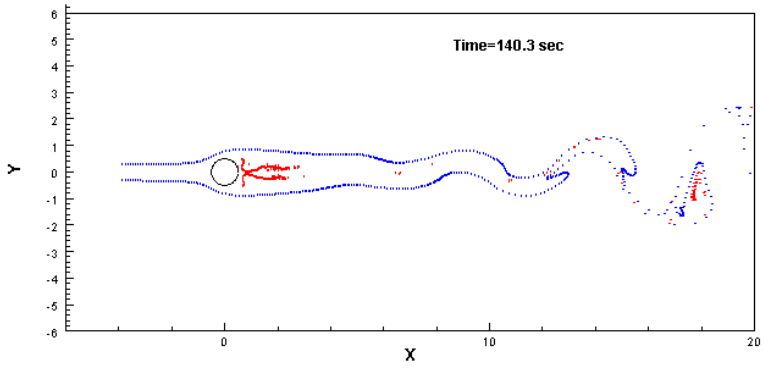

Figure 1.11: Particle traces for unsteady flow with electric field and magnetic field turned on at 120 s

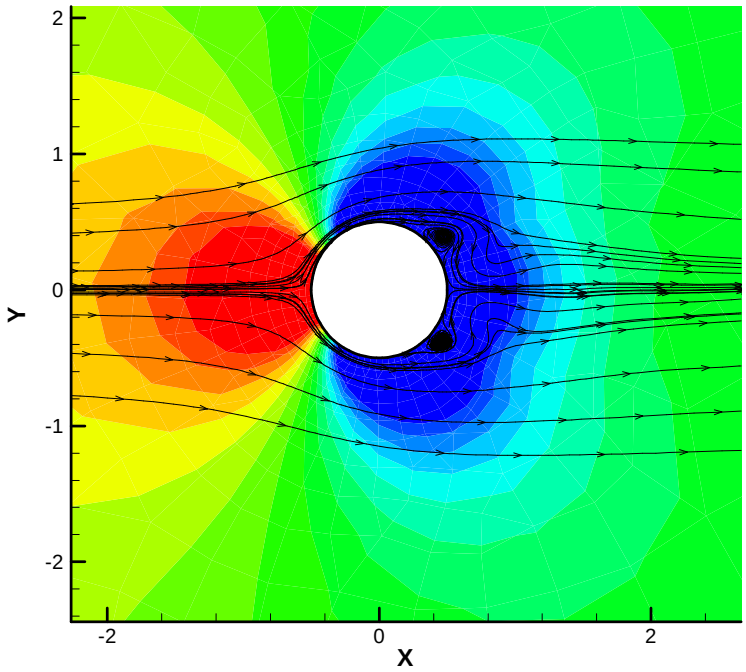

Figure 1.12: Pressure field and streamlines for Re=100 steady flow induced by electric field and magnetic field